EVLA Memo 137
Performance Tests of the EVLA K, Ka, and Q-Band Receivers

Rick Perley, Bob Hayward and Bryan Butler
NRAO

August 4, 2009

Abstract

Efficiency observations performed in January and February 2009 during clear dry weather with the EVLA receivers mounted on antenna #24 show excellent performance at K, Ka, and Q bands. System temperatures are well below project requirements, with mid-band values of 37, 43, and 58 K at K, Ka, and Q bands, respectively. Antenna efficiencies decline smoothly with increasing frequency, from a high of $\sim$ 55% at 18 GHz to $\sim$ 28% at 49 GHz, and are well fitted by a Ruze law, with a zero-frequency efficiency of 61% and surface roughness of 0.42 mm.

Antenna spillover temperatures at the zenith rise slowly with band, with values near 14, 16 and 18K at K, Ka, and Q bands. Spillover appears to be nearly constant at all three bands between 60 and 20 degrees elevation – this range is thus the best for determining atmospheric opacity through tip curves. All bands show a 1 – 2 degree rise in spillover at the zenith, presumably due to ground spillover seen at all lines of sight around the antenna reflector. Spillover at low elevations has a sharply band-dependent behavior: At K-band, a $\sim$ 4K excess is seen at all frequencies, while at Ka-band, there is very little change in spillover, even down to 8 degrees elevation. At Q-band, the behavior is notably different, with a $\sim$ 4K excess observed at the low-frequency end, and a $\sim$ 6K deficit at the high frequency end.

There were no peculiar changes in detected power like those noted in earlier tests which were performed while in the D-configuration. We conclude that these changes were caused by reflected ground radiation off adjacent antennas, and not by some inherent instability in the receivers.

1 Introduction

We have in two earlier memos (#103 and #125) given initial results on the sensitivity, efficiency, and spillover characteristics of the EVLA at the three highest frequency bands. In general, the results show that these receivers easily meet project requirements. However these tests – done on antenna #4 – were not complete, as we were unable to measure the antenna efficiencies at all bands with reasonable accuracy due to the primary calibrator Venus being ill-positioned at the time of those observations. In addition, two oddities in these results were noted:

1. There was an extra $\sim$5–8K of system temperature at all bands on antenna #4, constant in elevation and time, but not due to the receiver. Follow-up observations on antenna #2 showed this extra contribution was not present on that antenna, leading us to conclude that the excess on antenna #4 is due to thermal emission from its subreflector.

2. The system temperature seen on antenna #4, in all three bands, showed sudden rises and falls of typical amplitude $\sim$1K as the antenna was being moved in elevation or azimuth. Subsequent tests with this antenna and antenna #3 gave convincing evidence that this variable power

originates from ground radiation reflected by neighboring antennas – these observations were taken when the array was in the 'D'-configuration.

The new observations whose results are given in this memo were primarily driven by the need to determine accurate efficiency measurements at all three bands. Secondary drivers were the elucidation of the 'excess' spillover and apparent time-variable power seen in the earlier tests. By selecting an antenna whose location is distant from nearby antennas, and whose sensitivity is known from interferometry observations to be very good, we anticipated good results which would be indicative of the true capabilities of the electronics and antenna, and which would not be modified by adjacent antennas or sub-optimal electronics or deficiencies in the optics alignments. Antenna #24 was selected for these tests as it is a good performer at all bands and, being located at pad W32, is far from any other antenna.

Efficiency measurements require a source whose flux density is accurately known. By far the best source at these frequencies is the planet Venus, whose high brightness temperature and generally small angular diameter can provide up to 30K of antenna temperature – easily measured with our total power system. However, Venus, as an interior planet, is not always in a good position for efficiency observations for the VLA antennas – when near superior conjunction its flux density is only marginal for K-band observations, while near inferior conjunction its angular size of 60" is about equal to the FWHM of the Q-band primary beam. The optimal time for efficiency observations with the planet Venus is near maximum elongation when its angular size is about 30". Venus was in this position in January/February 2009.

2 Test Setup and Observations

The test setup was similar to that utilized for the tests reported in EVLA Memos #103 and #125. System total power was measured at the output of the T303 UX downconverter, using the setup schematically shown in Figure 1.

Observations were made at 15 frequencies – five at each of the three bands, chosen to span the full bandwidth of each receiver. Following our now well-established methodology, we performed a hot and cold load at each frequency to calibrate the system gain and determine the receiver temperature and calibration noise diode temperature, a sky dip to determine the atmospheric emission and opacity, and an observation of Venus to obtain the antenna aperture efficiency. To eliminate pointing issues, we observed Venus in a 7 x 7 or a 5 x 5 grid, with HPBW/4 spacing. All the Venus observations were taken within an hour of meridian transit, to minimize atmospheric emission and opacity variations.

Trial observations were taken on 10 Dec 2008 and 7 January 2009 for the purpose of testing the frequency setups and scripts. The observations which are analyzed in this memo were taken on 8 January, and 11 February 2009 under ideal weather, with clear skies, and light winds. On 8 January, Venus had an angular diameter of 23 arcseconds and transited at elevation of 46 degrees. On 11 February, its angular diameter was 34 arcseconds, and transited at an elevation of 61 degrees.

3 Calibration

Determination of the system temperature, receiver temperature, spillover temperature, and atmospheric emission and opacity utilized the same 'hot-cold' load method, plus antenna sky dips, as described in EVLA Memos #85, 90, and 103.

Estimates of the flux density of Venus were derived from established atmospheric emission mod-

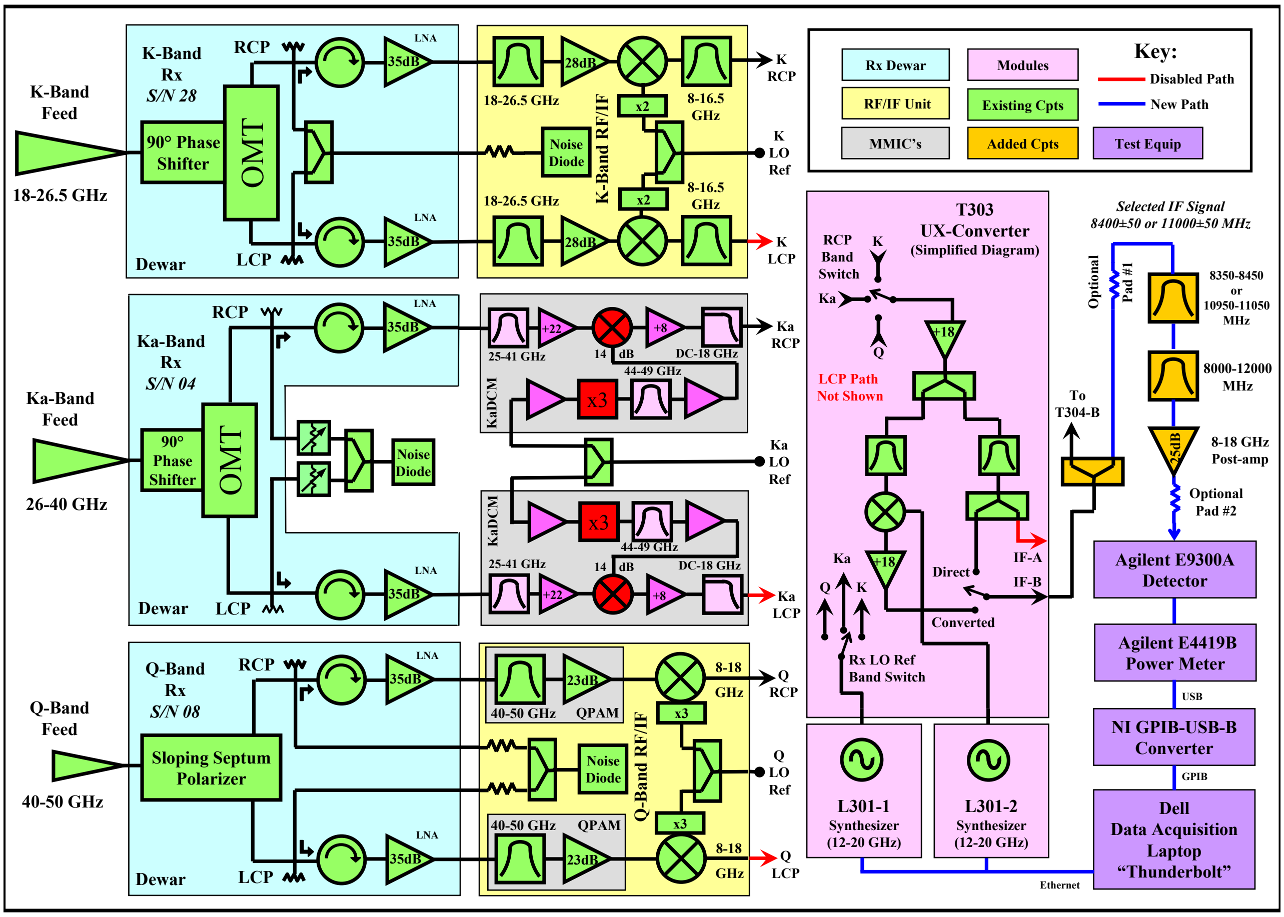

Figure 1: The setup used for these observations. The RF signals from the three receivers (blue boxes on the left) are block converted within the receiver down to an 8–18 GHz IF (yellow or grey boxes). This IF signal is sent to the T303 UX-converter (pink box) where a 4-GHz wide piece is selected by one of two paths ('direct' or 'converted'). The output signal was bandpass limited by a 100 MHz wide filter (gold boxes), and the power levels set with pads and post-amps to give a cold-sky level of approximately -35dBm needed for the power meter to give an accurately linear response over the 10 dB range between cold sky and hot load. The power measuring system (purple boxes) comprised an Agilent E3900A detector and E4419B power meter, whose data were recorded on a Dell Laptop using a Labview data acquisition program. By choosing the appropriate band switch setting, the test setup could be used to select between K, Ka, or Q band receivers using the EVLA control system. The splitter at the output of the T303 allows the EVLA interferometer signal path and the total power measurement system to operate in parallel.

els[1]. The modelled flux was then adjusted by atmospheric opacity and primary beam attenuation, then converted to antenna temperature for comparison to the observed power.

4 Results

4.1 Calibration

Calibration was accomplished using the same method as described in Memo #103. In short, the known temperatures of the hot and cold loads enable calibration of the system gain, thus permitting conversion of the measured system power to temperature units, and calibration of the internal noise

[1]Butler, B.J., Steffes, P.G., Suleiman, S.H., Kolodner, M.A., and Jenkins, J.M., 'Accurate and Consistent Microwave Observations of Venus and their Implications', Icarus, **154**, 226-238, 2001

diode and receiver temperatures. The sky dip data were fitted with an atmospheric emission model to allow separation of the elevation-dependent (atmospheric emission) and constant (spillover and receiver) components. From the latter, the known receiver component is subtracted to provide the spillover contribution.

In our past tests, the three component observations (hot/cold, sky dip, and Venus observation) were grouped for each frequency. The advantage of this is that variations in receiver gain are minimized, and the hot/cold calibration can more safely be applied to all tests. In these observations, our goal of completing 15 separate frequencies in one day required the tests to be grouped by type, rather than frequency. Hence, all 15 hot/cold determations were done together, followed by the 15 raster scans of Venus, and finally the 15 sky dips. Because the receiver gain is likely to vary over the long time required (the entire operation took 7 hours), we are dependent upon the stability of the internal noise diode – which was fired for each of the 45 components of these tests – for our calibration. Excellent evidence for the stability of the noise diode can be obtained from comparison of the derived noise diode calibration temperatures for frequencies observed on the three observation dates. These results are shown in Table 1. Stability of better than $\sim$3% is typical. Note also the stability in the receiver and system temperatures.

4.2 Atmospheric Emission and Spillover Temperature

Sky dips were made at all frequencies in order to determine the variation with elevation of the total system temperature. As described in previous memos, we fitted atmospheric emission curves which take account of both the atmospheric emission and 2.7K CMB radiation. The model separates the atmospheric contribution from spillover contribution through the former's known variation with elevation. This separation works well if the variation of spillover with elevation is much smaller than that of the atmospheric component. A good separation is important because the atmospheric component provides us with an estimate of the opacity, which is needed in the determination of the efficiency.

Examination of the tip power indicates that spillover variation exceeds that of the atmosphere at high elevations ($E > 60$), and at low elevations ($E < 20$). Hence, we solved for the atmospheric terms over the elevation range of 20 through 60 degrees, where the variation in spillover seems to be constant. The data in this elevation range were fitted with the following expression (see EVLA Memo #103 for justification):

$$T_{sys} = T_r + \epsilon[T_{cmb}e^{-\tau_0 \sec(z)} + T_{em}(1 - e^{-\tau_0 \sec(z)})] + (1 - \epsilon)T_{gnd}. \tag{1}$$

The first term on the RHS is the constant receiver component, and is known from the hot/cold load measurements. The second term is the atmospheric component. The last term is the (assumed non-varying) spillover contribution[2], whose origin will be both from the ground and the antenna itself. T_{cmb} is the cosmic background radiation, T_{gnd} is the effective ground radiation temperature, which we take to be 280K. T_{em} is the effective atmosphere radiation temperature, which is related to the ground air temperaure T_s by (Bevis et al. 1992)

$$T_{em} = 70.2 + 0.72T_s \tag{2}$$

For our January observations, this is 274K, while for the February observations it is 270K. We solve for τ_0, the vertical atmospheric opacity, and ϵ, which represents the fraction of the total antenna temperature which enters through the main beam and its nearby sidelobes (and hence has the indicated variation with elevation). Note that there is no need for an earth curvature term in the opacity, as this is negligible at the elevations employed. The results giving the atmospheric opacity,

[2] a more sophisticated model would include spatially variant forward and reverse spillover

Freq MHz	Date K	T_{cal} K	T_r K	T_{90} K	T_{cal} K	T_r K
18440	08Jan09	1.44	27.4	48.8	1.40	22.7
18952	07Jan09	2.06	20.0	42.0	2.09	18.6
18952	08Jan09	2.08	18.8	43.0		
23560	07Jan09	1.61	11.8	39.6	1.62	11.9
23560	08Jan09	1.57	11.0	39.8		
25608	07Jan09	1.54	11.4	36.2	1.52	12.0
25608	08Jan09	1.58	12.3	39.5		
26120	08Jan09	1.49	17.5	42.4	1.43	15.5
26232	08Jan09	5.13	33.3	55.5	4.88	28.3
28024	07Jan09	6.09	18.6	42.1	5.86	17.8
28024	08Jan09	6.16	19.3	42.2		
33160	10Dec08	5.56	16.0	41.1	5.61	16.3
33160	07Jan09	5.53	15.7	42.3		
33160	08Jan09	5.69	16.3	42.9		
38064	07Jan09	3.73	23.7	50.8	3.12	28.4
38064	08Jan09	3.74	23.6	50.3		
39600	08Jan09	2.35	38.5	66.7	2.28	38.4
40368	07Jan09	7.06	29.6	62.7	6.81	30.7
40368	08Jan09	7.23	29.5	65.9		
40368	11Jan09	7.40	30.7	60.4		
41136	08Jan09	3.64	24.1	58.1	3.62	26.0
41136	11Feb09	3.82	24.1	54.5		
43440	07Jan09	5.87	25.0	60.8	5.69	28.3
43440	08Jan09	6.00	24.3	64.3		
43440	11Feb09	6.18	25.0	58.5		
48048	08Jan09	3.95	29.6	88.8	3.21	31.6
48048	11Feb09	4.26	30.8	79.2		
49584	07Jan09	2.43	39.7	104.7	2.45	39.8
49584	08Jan09	2.46	39.7	105.5		
49584	11Feb09	2.63	41.8	98.0		

Table 1: The noise diode temperatures, receiver temperatures, and system temperatures at the zenith on the three observing days (plus an observation in Dec 2008 at 33160 MHz). The weather conditions were very similar on all three days. The repeatability of the noise diode temperatures is better than 3% at K and Ka bands. There is evidence that the Q-band noise diode temperature is slowly rising over time. The receiver temperatures appear to be more stable than the noise diode. The right-hand pair of columns show the lab measurement of the noise diode and receiver temperatures. The origin of the notably reduced system temperatures on 11 February remains mysterious...

spillover temperature ($T_{sp} = (1-\epsilon)T_{gnd}$), and total system temperature (at elevation = 90) are given in Table 2.

5 Efficiency

The efficiency observations utilized the planet Venus, which was ideally positioned at the time – near maximum eastern elongation, and an elevation near 45 degrees at meridian transit for the January observations, and near 61 degrees in February. The planet subtended an angle of about 23

Freq MHz	τ	T_{sp} K	T_{sys} K	τ	T_{sp} K	T_{sys} K
18440	.0183	13.2	48.8			
18952	.0214	15.1	43.0			
23560	.0431	14.3	39.8			
25608	.0270	13.4	36.5			
26120	.0271	14.3	42.4			
26232	.0251	12.0	55.5			
28024	.0252	12.9	42.2			
33160	.0283	16.2	42.9			
38064	.0311	15.7	50.3			
39600	.0412	14.8	66.7			
40368	.0517	18.5	65.9	.049	13.2	60.4
41136	.0512	17.6	58.1	.052	13.8	54.5
43440	.0695	19.9	64.3	.067	13.8	58.5
48048	.142	23.0	88.8	.133	15.1	79.2
49584	.175	22.4	105.5	.164	14.3	98.0

Table 2: The derived vertical atmospheric opacity and spillover temperatures, with the January results on the left, and the February results on the right. The difference in the Q-band results are due to reduced spillover, but we do not understand the origin.

arcseconds in January, and 34 arcseconds in February, requiring only minor corrections for antenna primary beam resolution.

The maximum antenna temperature noted in each raster was calibrated via the known noise diode value. The Venus antenna temperature was then compared to that expected from the planet, utilizing a model accounting for Earth's atmospheric opacity, the partial resolution of the planet by the antenna beam and limb darkening of the planet.[3]

The derived efficiencies are shown in Table 3.

In an often-cited paper ('Antenna Tolerance Theory – A Review', Proc. IEEE, 54, #4, 633-640, April 1966), Ruze noted that for the efficiency of a paraboloid antenna due to a surface rms error σ declines with frequency as

$$\epsilon = \epsilon_0 e^{-\left(\frac{4\pi\epsilon}{\lambda}\right)^2}. \tag{3}$$

Ruze notes that this simple formula holds for any smooth aperture illumination and is valid for losses of up to several dB provided the surface errors are uniformly distributed over the aperture. We have fitted this law to our efficiency data, with the results shown in Fig. 2. The fit is very satisfactory, with a 'zero-frequency' intercept of 61% – about the value expected due to blockage and the aperture illumination weighting. The panel roughness of 0.42mm is in agreement with expectations.

6 Spillover

As noted above, the separation of the atmospheric component from others depends on knowledge of the elevation dependence of these components. The variation of the atmospheric component is well understood, but that of the ground spillover is not known at all. We have separated these in our

[3]Butler, B.J., Steffes, P.G., Suleiman, S.H., Kolodner, M.A., and Jenkins, J.M., 'Accurate and Consistent Microwave Observations of Venus and their Implications', Icarus, **154**, 226-238, 2001

Freq MHz	τ	FWHM arcmin	T_b K	F_r	F_d Jy	T_{Venus} K	T_{obs} K	ϵ
18440	.0259	2.41	537	.992	51.8	9.21	4.6	0.50
18952	.0303	2.39	533	.992	53.9	9.55	5.45	0.57
23560	.0610	1.93	500	.988	75.3	13.4	7.00	0.52
25680	.0382	1.77	489	.985	89.0	15.8	8.29	0.52
26120	.0383	1.74	486	.985	92.5	16.4	7.92	0.48
26232	.0355	1.73	485	.985	93.9	16.8	8.13	0.48
28024	.0356	1.62	476	.983	105	18.7	9.00	0.48
33160	.0400	1.37	453	.976	139	24.6	10.67	0.43
38064	.0440	1.91	437	.968	174	30.9	10.94	0.35
39600	.0583	1.15	432	.966	182	32.4	11.00	0.34
40368	.057	1.12	430	.918	423	75.2	27.9	0.37
41136	.0604	1.10	428	.916	434	77.2	29.0	0.38
43440	.077	1.04	422	.906	463	82.4	31.2	0.38
48048	.154	.944	411	.887	495	88.0	28.3	0.32
49584	.189	.915	407	.880	497	88.3	25.0	0.28

Table 3: Showing the results of the efficiency measurements. The K and Ka band data are from the January observations, the Q band data from the February observations. Errors should not exceed 0.05, except at 18440 MHz, where the data were corrupted by an unknown variability. The observation at 18440 MHz is very uncertain due to a variable gain during the measurement. The columns are: (1) Frequency in MHz, (2) actual opacity, (3) antenna beamwidth, (4) mean planet brightness temperature, (5) beam dilution factor, (6) modelled flux, accounting for opacity and beam resolution, (7) antenna temperature due to Venus, presuming $\epsilon = 1$, (8) observed antenna temperature, (9) antenna efficiency.

datasets by carefully selecting an elevation range where the non-atmospheric component appears to be quite constant – essentially, the atmospheric model fits the data within this range very well.

Some idea of the limitations in our procedure can be found by using the values of opacity and spillover found over the limited elevation range, and deriving the difference between the model and the data over the full elevation range. The results are shown in Figure 3.

Figure 3 shows some very curious behavior – clearly differentiated by band – which has shown up in our earlier work. We note these below.

- All frequencies at all bands show an excess of ~1 K at the zenith compared to an elevation of 50 degrees. This is presumably due to extra (reverse) spillover around the limb of the main reflector, as all sight lines from the subreflector past the limb terminate at the ground when the antenna is pointed at the zenith. Sightlines past the antenna limb at the top of the dish terminate on the sky beginning at an elevation of 70 degrees.

- The K-band observations at all frequencies (solid lines) show a similar excess over the atmospheric starting at an elevation of about 20 degrees, and reaching about 4K at elevations below 12 degrees. This is presumed to be due to (forward) spillover of the primary horn illumination about the subreflector, whose diameter subtends an angle of 18 degrees as seen by the horn.

- By contrast, all Ka-band observations (dashed lines) show little or no excess over the atmospheric model, suggesting that primary horn spillover past the subreflector is negligible.

- The most curious behavior is seen at Q-band (dash-dot lines) where a low-elevation excess is seen at the lower frequencies (much like at K-band), while a deficiency is seen at high frequencies. While it is tempting to think that opacity and earth curvature effects are responsible for

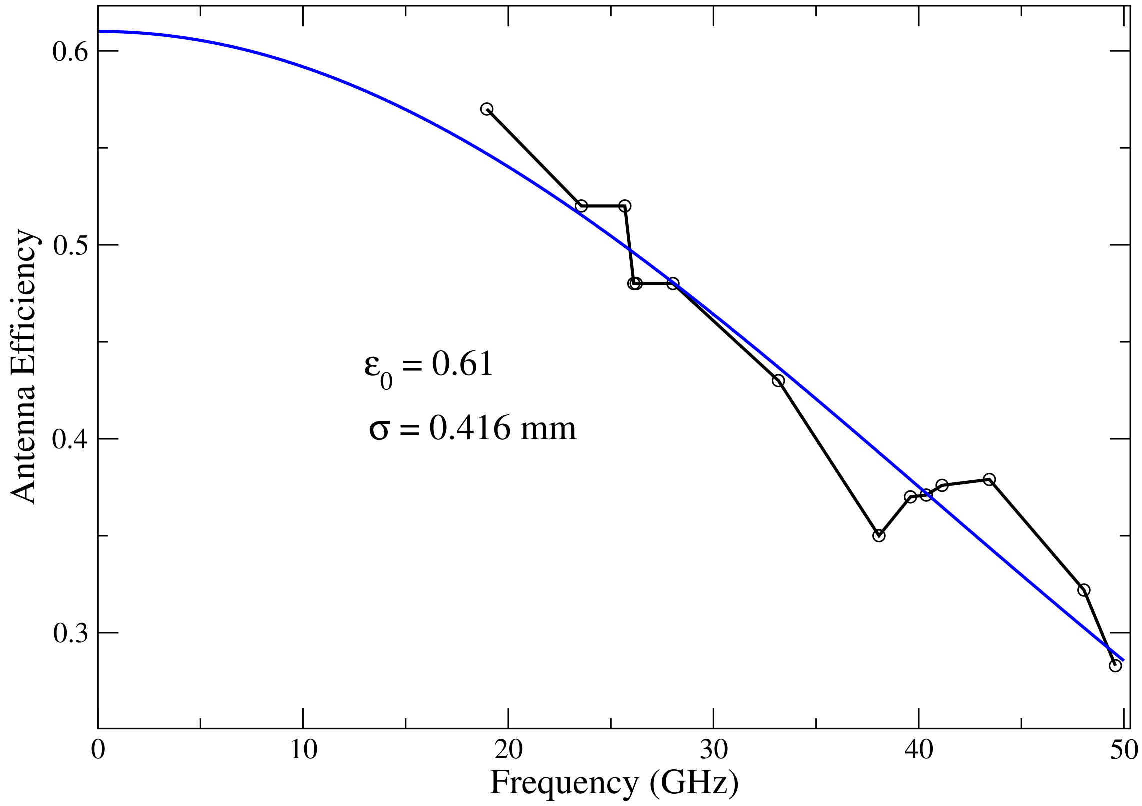

Figure 2: Showing the fit of the efficiency to a Ruze model

this deficiency, our simple model returns physically impossible results when these parameters are included.

7 Conclusions and Discussion

The most important conclusion from this work is that the antenna performance at all three bands easily exceeds the EVLA Project requirements. Table 4 summarizes the results and the requirements. The project requirements for antenna sensitivity are given for mid-band, except at Q-band, where due to atmospheric opacity the requirements are spelled out for a low (43 GHz) and high (48 GHz) frequency, as shown in the table.

It is seen that the actual antenna/receiver performance easily exceeds the project requirements at these bands. One note of caution should be added here – we have taken great pains to make these measurements in the best possible weather, and using a raster scanning methodology which guaranteeds on-axis measurements. Regular observing conditions – particularly at the highest frequencies, and at frequencies near 23 GHz where terrestrial water vapor can add considerable power – will rarely equal what we have striven to obtain, so that obtained sensitivities will rarely meet the values shown. However, we should be within a few tens of percent of these values in good weather.

The peculiar power fluctuations reported in Memos #103 and #125 were not seen in these observations, supporting our conclusion that these fluctuations were due to ground radiation reflected off nearby antennas. Fortunately, this redirected ground radiation accounts for only a few K, except when heavy shadowing is occuring – in which case the data will be flagged in any event.

Excess spillover is usually seen at these bands at elevations below 20 degrees. This is expected

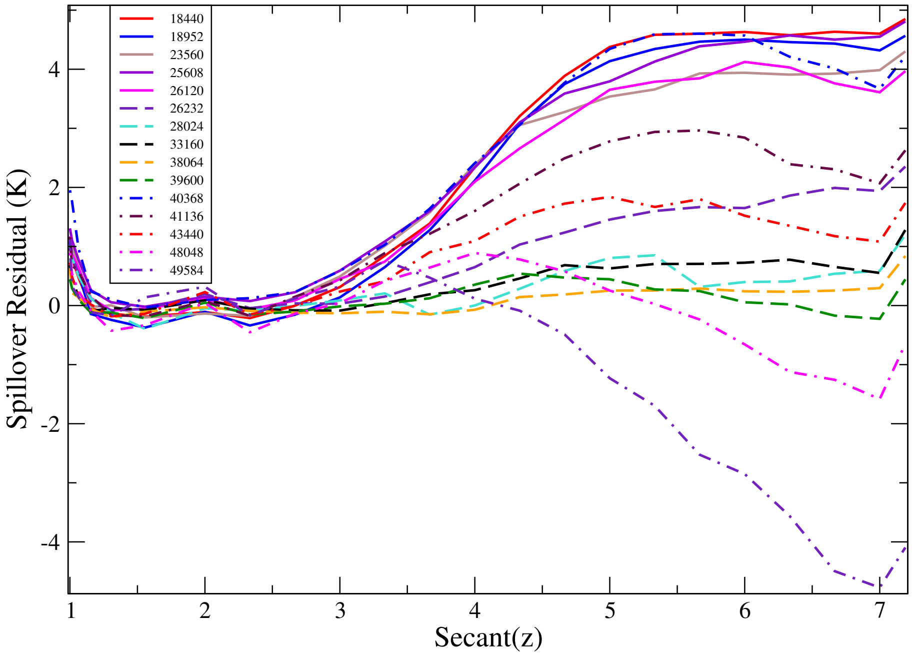

Figure 3: Showing the residual between the atmospheric model and the observed data. If the atmospheric model is correct, the values shown represent the variation in the spillover with elevation, relative to the value determined over the model range (60 to 22 degrees). The five K-band frequencies all behave in identical manner – an excess at very low elevations, compatible with excess spillover from the forward direction as the ground becomes in view. However, at Ka-band, there is little evidence for any change in spillover, even at the lowest elevations. At Q-band, the situation changes dramatically from an low-elevation excess at the low frequencies, to an distinct low-elevation deficit at the highest frequencies. All of the variations can be fitted well by a model incorporating earth curvature – however the values required for the atmospheric scale height are far too large to be reasonable.

behavior, but is of little consequence, as the additional power is generally less than 4K, and in any event, observing at such low elevations is generally discouraged for other reasons – increased opacity diminishing the signal power, and much degraded resolution due to foreshortening.

Freq MHz	T_{sys} K	ϵ	T_{sys}/ϵ K	SEFD Jy	SEFD(req) Jy
18440	49	.50	98	550	
18952	43	.57	75	420	
23560	40	.52	77	430	650
25680	37	.52	71	400	
26120	42	.48	88	495	
26232	56	.48	116	650	
28024	42	.48	88	495	
33160	43	.43	100	560	760
38064	50	.35	142	800	
39600	67	.34	197	1110	
40368	66	.37	178	1000	
41136	58	.38	153	860	
43440	64	.38	168	944	1220
48048	88	.32	275	1550	2760
49584	106	.28	380	2130	

Table 4: Showing the observe zenith system temperature, derived efficiency, the resulting effective system temperature (T_{sys}/ϵ), and System Equivalent Flux Density (the flux density of a source which doubles the system temperature). The EVLA Project requirement for SEFD is shown in the right-most column.